CHALMERS
UNIVERSITY OF TECHNOLOGY

1060 nm Single-Mode VCSEL and Single-Mode Fiber Links for Long-Reach Optical Interconnects

Citation for the original published paper (version of record):
Simpanen, E., Gustavsson, J., Larsson, A. et al (2019). 1060 nm Single-Mode VCSEL and Single-Mode Fiber Links for Long-Reach Optical Interconnects. Journal of Lightwave Technology, 37(13): 2963-2969. http://dx.doi.org/10.1109/JLT.2019.2908249

1060 nm Single-Mode VCSEL and Single-Mode Fiber Links for Long-Reach Optical Interconnects

1060 nm Single-Mode VCSEL and Single-Mode Fiber Links for Long-Reach Optical Interconnects

Ewa Simpanen, *Student Member, IEEE*, Johan S. Gustavsson, Anders Larsson, *Fellow, IEEE*, *Fellow, OSA*, Magnus Karlsson, *Senior Member, IEEE*, *Fellow, OSA*, Wayne V. Sorin, Sagi Mathai, Michael R. Tan and Scott R. Bickham

***Abstract*—We investigate the use of a 1060 nm single-mode vertical-cavity surface-emitting laser (VCSEL) and a 1060 nm single-mode fiber as a competitive single-mode technology for cost and power efficient long-reach optical interconnects. Error-free transmission (BER < 10^{-12}) over 2 km is demonstrated at bitrates up to 40 Gbps under OOK-NRZ modulation, without equalization, forward-error correction, or other forms of digital signal processing. The VCSEL is extensively characterized with respect to its static and dynamic performance, including the power-voltage-current characteristics, spectral characteristics, beam divergence, modulation response, relative intensity noise, and frequency chirp. The measured dependence of power penalty on fiber length is consistent with an analysis of chirp-induced pulse compression and broadening along the negative chromatic dispersion fiber.**

***Index Terms*—Optical interconnections, single-mode, vertical-cavity surface-emitting lasers.**

I. Introduction

DATA CENTERS use optical interconnects (OIs) for efficient transport of large amounts of data between server racks. For shorter reach, less than 300 m, 850 nm multimode (MM) solutions currently dominate the market, using MM GaAs-based vertical-cavity surface-emitting lasers (VCSELs) as light sources, together with multimode fiber (MMF) [1] [2]. The higher level networks in large-scale data centers use single-mode (SM) technology to accommodate the need for longer reach (up to ~2 km) [3], with transceiver solutions based on 1310 and 1550 nm Si-photonic [4] and/or InP [5] [6] technologies. Parallel single-mode (PSM) and wave division multiplexing (WDM) solutions are being developed and standardized for 400 Gbps and higher aggregate OI capacity [3] [7].

Much of the success of the 850 nm MM VCSEL technology stems from its cost and power efficiency, but reach is fundamentally limited by the high fiber chromatic dispersion and attenuation at this wavelength [2] [3]. This raises the question whether extending the wavelength towards the upper limit of the GaAs-based material system (~1100 nm [8]), where optical fiber properties are much improved with respect to 850 nm, could bring the same advantages in terms of cost and power efficiency to long-reach SM OIs as the GaAs-based VCSEL technology has done to short-reach MM OIs. This would require high-performance longer wavelength SM VCSELs on GaAs as well as single-mode fiber (SMF) with a cutoff wavelength shorter than that of the standard SMF.

For the purpose of extending the wavelength without compromising reliability [8] [9], GaAs-based VCSELs at 1060 nm have been developed. At this wavelength, fiber chromatic dispersion is one-third and attenuation is half compared to 850 nm [2]. Furukawa has demonstrated 20 GHz bandwidth oxide-confined 1060 nm MM VCSELs with double intra-cavity contacts and a dielectric top distributed Bragg reflector (DBR), enabling 25 Gbps OOK-NRZ transmission over 1 km of 1060 nm optimized MMF [10]. With VCSELs from Furukawa, Georgia Tech demonstrated 50 Gbps PAM-4 transmission over 300 m of wideband MMF using pre-emphasis and forward error correction (FEC) [11]. Hewlett Packard Enterprise recently demonstrated 25 Gbps OOK-NRZ and 50 Gbps PAM-4 transmission over 2 km of standard SMF with a 1065 nm SM VCSEL using FEC [12].

Our 1060 nm VCSELs (MM and SM) have previously been investigated in terms of the most basic performance characteristics and transmission capacity back-to-back (BTB) and over 1060 nm optimized MMF [13]. The VCSEL technology employs weak transverse confinement of the optical fields and strong transverse confinement of the current to promote SM operation. With SM VCSELs, BTB transmission up to 50 Gbps has been demonstrated [14]. Preliminary results from transmission over 1060 nm SMF

This work is supported by the Hewlett Packard Enterprise Innovation Research Program, the Swedish Foundation for Strategic Research, and the Swedish Research Council (Grant No. 2016-06077).

E. Simpanen, J. S. Gustavsson, A. Larsson, and M. Karlsson are with Photonics Laboratory, Department of Microtechnology and Nanoscience, Chalmers University of Technology, SE 41296 Gothenburg, Sweden (e-mail: ewa.simpanen@chalmers.se; johan.gustavsson@chalmers.se; anders.larsson@chalmers.se; magnus.karlsson@chalmers.se).

W. V. Sorin, S. Mathai, and M. Tan are with Hewlett Packard Enterprise, 1501 Page Mill Road, Palo Alto, CA 94304-1123, USA (e-mail: wayne.sorin@hpe.com; sagi.mathai@hpe.com; mike.tan@hpe.com).

S. Bickham is with Corning Research and Development Corporation, 1 Science Center Drive, Painted Post, NY 14870, USA (e-mail: bickhamSR@corning.com).

(40 Gbps OOK-NRZ over 2 km) were presented in [15]. Here, we extend this study by more extensive characterization of the SM VCSEL, also in terms of beam divergence, relative intensity noise, and frequency chirp. We additionally investigate the alignment tolerance to the SMF and analyze the chirp-induced power penalty and its dependence on fiber length through measurements and a numerical analysis. The 1060 nm SMF used is a prototype fiber manufactured by Corning.

Compared to MM technologies, any SM transceiver technology (implemented for the purpose of reach extension) suffers from increased complexity and cost related to alignment and assembly. This is true also for SM OIs based on 1060 nm SM VCSELs and SMFs. However, the cost benefit of GaAs-based SM VCSELs is the same as that of GaAs-based MM VCSELs (similar fabrication cost) and the design and production cost of the 1060 nm SMF is similar to that of other commercial fibers that are manufactured in volume.

II. 1060 nm SM VCSEL Design

The 1060 nm VCSEL design [14] is partly based on a previous 850 nm high-speed oxide-confined VCSEL design [16] with strong transverse current confinement. Together with the weak transverse optical confinement used in the 1060 nm design, this enables SM operation with a relatively large oxide aperture.

The epitaxial structure, grown by metal-organic chemical-vapor deposition on undoped GaAs (at IQE), consists of an active region between a top p-doped AlGaAs/GaAs DBR and a bottom n-doped AlGaAs/GaAs DBR. The DBRs have graded composition interfaces and are modulation doped for efficient transport of carriers across the interfaces and low internal optical loss. The lower part of the bottom DBR employs binary AlAs/GaAs pairs for low thermal impedance.

The active region has three strained InGaAs quantum wells (QWs) with high In-content for wavelength extension. The QWs are separated by partially strain-compensating GaAsP barriers, resulting in net compressive strain in the QWs for high differential gain. The length of the optical cavity is half a wavelength for strong longitudinal optical confinement and high field intensity in the QWs.

Carriers and photons are confined in the transverse direction by two primary oxide apertures in the top DBR (Fig. 1). The primary apertures are thin and positioned at optical field nodes for weak guiding and large transverse mode size. They are also positioned close to the active region for strong transverse current confinement, which together with the large mode size promotes SM operation. The large mode size also reduces the beam divergence. Four secondary oxide layers above the primary help reduce the capacitance residing from charge stored over the oxide layers.

Standard processing techniques are used for VCSEL fabrication. The full-semiconductor device is planarized with BCB to reduce the pad capacitance. As a final step in the fabrication, the thickness of the uppermost layer of the top-DBR, and therefore the top-DBR reflectivity, is tuned to set the cavity photon lifetime for a sufficiently damped but high-bandwidth modulation response to avoid excessive timing jitter and intersymbol interference [17].

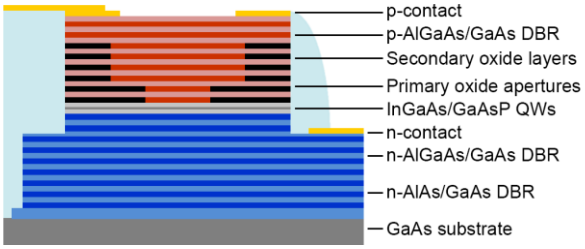

Fig. 1. Schematic of the 1060 nm SM VCSEL design, specifying the material compositions of the active region, top p-DBR and bottom n-DBR. The placement of the p-contact, intra-DBR n-contact, and oxide apertures are also indicated. For strong transverse current confinement, the lowest primary oxide aperture is placed in the mirror pair closest to the active region.

A VCSEL with a 4 µm primary oxide aperture diameter was found to be strongly SM. Therefore, all measurements (at room temperature) in the following sections are for a VCSEL with this aperture size.

III. Static Performance

The optical output power and voltage as a function of current are shown in Fig. 2. Power was measured with a calibrated large area Ge-photodiode. The threshold current is 0.15 mA and the slope efficiency is 0.5 W/A, whereas the maximum power is 2.3 mW at thermal rollover. The low threshold current can be attributed to the strong confinement of carriers and the small aperture. At a bias current of 4 mA, which was found to be the optimum current for data transmission, the output power is 1.7 mW, the voltage is 2.8 V, and the differential resistance is 250 Ω.

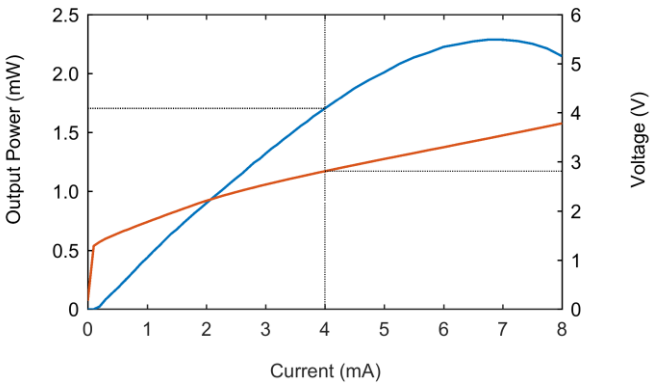

Fig. 2. Optical output power versus current (blue, left), and voltage versus current (red, right) for the 4 µm aperture 1060 nm VCSEL. Indicated is the bias current of 4 mA used for data transmission, where the output power and voltage are 1.7 mW and 2.8 V, respectively.

Emission spectra were recorded by butt-coupling the VCSEL to a short OM4 fiber connected to an ANDO AQ6317 optical spectrum analyzer. Fig. 3 shows SM emission with a suppression of higher order transverse modes of ~50 dB at all currents. At 4 mA, the wavelength of the fundamental mode is 1065.3 nm. When increasing the current from 3 to 5 mA, a 2.1 nm redshift is observed due to current-induced self-heating.

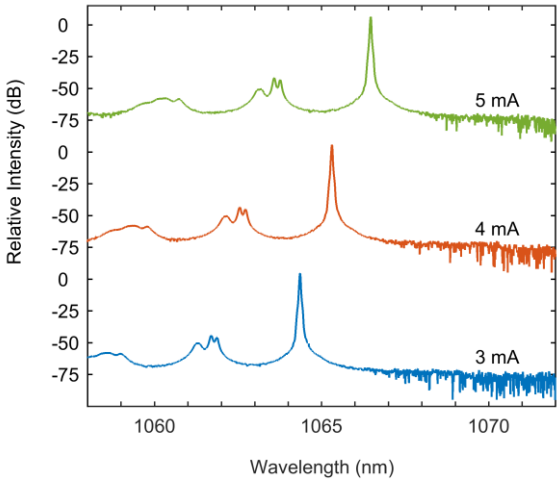

Fig. 3. Spectra measured at 3, 4 and 5 mA, with prominent SM emission (higher order mode suppression ~50 dB).

Beam profiles were measured by angular scanning of the Ge-photodiode behind a small pinhole through the beam, at a long distance (in the far-field) from the VCSEL. The beam profile, shown in Fig. 4, was fitted to that of a Gaussian beam. The $1/e^2$ full-width beam divergence was determined to be 29.6° at 4 mA, which corresponds to a beam waist diameter of 2.6 µm at the VCSEL surface (near-field). The relatively small beam divergence is attributed to the weak transverse optical confinement and large mode size. The divergence angle increased by 2.2° when the current was increased from 1 to 5 mA due to thermal lensing. Fig. 4 also shows the 2D beam cross-section captured by positioning a diffusive glass plate in the far-field and imaging the opposite side of the plate with a Spiricon SP928 camera from Ophir Optronics Solutions.

IV. Dynamic Performance

For data transmission, the VCSEL dynamics, including the modulation response and the intensity noise, are of greatest importance. For SM VCSEL and SMF links, also the frequency chirp is of importance since, together with the chromatic dispersion in the fiber, it determines the amount of pulse broadening and/or compression along the fiber. Therefore, all these parameters were measured for the 4 µm aperture SM VCSEL.

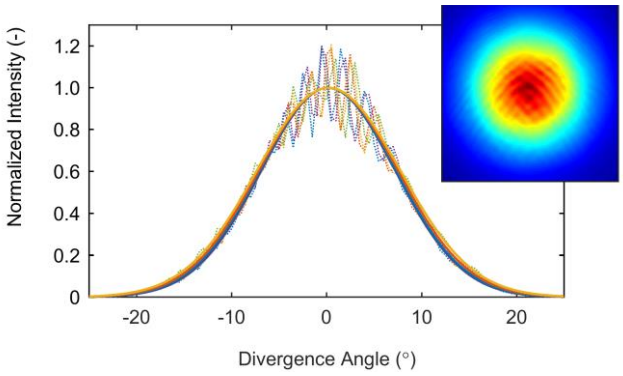

Fig. 4. Beam profiles measured at 1, 2, 3, 4 and 5 mA with Gaussian fits. The ripple is caused by interference in the imaging system. Inset: 2D beam cross-section at 4 mA, showing a highly circular beam.

A. Small-Signal Modulation Response

The modulation response was measured with a 67 GHz Rohde & Schwarz ZVA vector network analyzer and a 28 GHz Picometrix DG-32xr photodetector. The results, together with fits of the conventional VCSEL transfer function [18], are shown in Fig. 5 where the measured small-signal modulation response at different currents is displayed.

The -3 dB modulation bandwidth is consistently high at currents above 3 mA, where the modulation response is damped and relatively flat, reaching its maximum bandwidth of 22.5 GHz at 5.4 mA. At 4 mA, the modulation bandwidth is 22.1 GHz. The resonance tends to be more damped in a SM VCSEL compared to a MM VCSEL, due to the high photon density in the center of the device causing strong spatial hole burning and carrier diffusion [19]. An indication of the increase of damping with resonance frequency is given by the K-factor, which for this VCSEL was extracted to be 0.23 ns. The SM VCSEL with a small oxide aperture and strong transverse carrier confinement also has a small effective gain volume, which gives rise to a high D-factor (which quantifies the increase of resonance frequency with current), extracted to be 16 GHz/mA$^{1/2}$. The parasitic pole frequency is close to 19 GHz, indicating that primarily parasitics and thermal effects due to self-heating are limiting the modulation bandwidth.

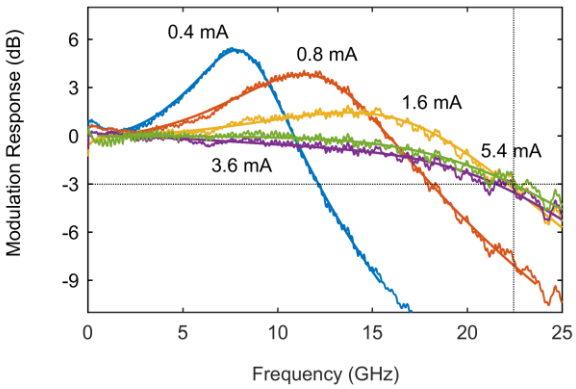

Fig. 5. Small-signal modulation response (S21) at 0.4, 0.8, 1.6, 3.6 and 5.4 mA bias current, and corresponding three-parameter transfer function fits, showing a maximum bandwidth of 22.5 GHz at 5.4 mA.

B. Relative Intensity Noise

Measurements of the VCSEL relative intensity noise (RIN) were performed using a short butt-coupled OM4 fiber connected to a 25 GHz New Focus 1414 MM photodetector. The fiber was tilted at a small angle to avoid optical feedback to the VCSEL, which could enhance RIN. The noise spectral density of the received signal was measured using a 50 GHz Agilent PXA N9030A signal analyzer. A 25 GHz bandwidth, 27 dB gain low-noise amplifier (SHF 115AP) was used to bring the signal above the noise floor of the signal analyzer. The total noise spectrum (RIN, shot noise, and thermal noise) was first recorded with the VCSEL biased at different currents. The thermal noise spectrum was then recorded with

the VCSEL turned off.

RIN, defined as the mean square of the optical intensity fluctuation over the square of the average optical power, was calculated from the measured electrical noise power spectral densities [20] as

$$RIN(f) = \frac{\sigma_{tot}(f) - \sigma_{th}(f)}{I_0^2 \cdot R_L} - \sigma_{shot}, \quad (1)$$

where σ_{tot} is the total system noise, σ_{th} is the thermal noise, σ_{shot} ($=2q/I_0$) is the shot noise, I_0 is the measured detector dc photocurrent, and R_L is the detector load resistance. All noise powers have their reference point at the detector output and are corrected for the frequency response of the amplifier.

The spectra in Fig. 6 show the frequency dependence of the sum of RIN and shot noise up to currents of 6 mA. As expected, the intensity noise is strongest at the resonance frequency and is reduced with current because of the increasing photon density in the active region. At high currents, the intensity noise approaches the shot noise level, as expected for a SM VCSEL. At a current of 4 mA, the average RIN is -157 dB/Hz, which will give negligible penalty for 40 Gbps OOK transmission [21]. Compared to MM VCSELs, SM VCSELs are free from mode partition noise and the performance of SM VCSEL and SMF links do not suffer from the noise enhancement that occurs in MM VCSEL and MMF links due to mode selective coupling [22]. SM lasers are, however, more susceptible to RIN enhancement due to optical feedback [23].

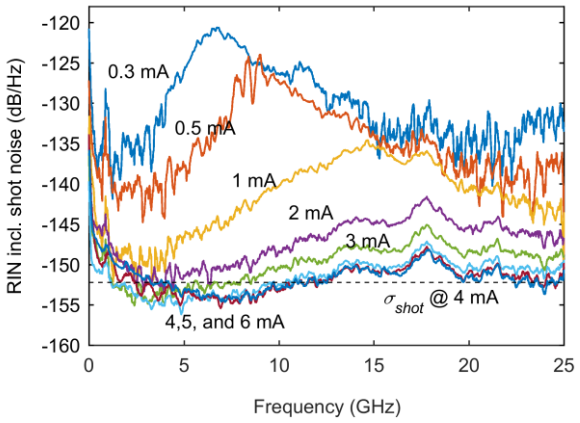

Fig. 6. RIN, including shot noise calculated from detector photocurrent, measured at 0.3, 0.5, 1, 2, 3, 4, 5 and 6 mA bias current. The dashed line represents the 4 mA shot noise level at –152 dB/Hz.

C. Frequency Chirp

As the VCSEL undergoes direct current modulation, the photon density varies and momentary changes in the carrier population induce fluctuations in the refractive index of the active region. This gives rise to variations in the laser frequency (or wavelength) that broaden the VCSEL spectral width and lead to pulse broadening or compression along the dispersive fiber.

The time-resolved frequency chirp was measured using a Fabry-Perot etalon as an optical frequency discriminator [24]. The etalon used in these experiments is a custom designed fiber-coupled etalon from Micron Optics (FFP-I) with a free spectral range (FSR) of 300.72 GHz, a finesse of 2.5, and mirror reflectivities (R) of 30%. The transmission characteristics of the etalon are shown in Fig. 7. By temperature tuning the laser wavelength to either the positive or the negative slope of the transmission curve, frequency fluctuations are converted to intensity fluctuations.

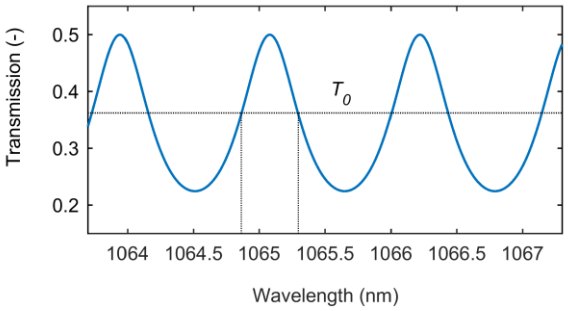

Fig. 7. Etalon transmission versus wavelength calculated using FSR = 300.72 GHz and mirror reflectivity of 30%. The mean transmission T_0 is indicated, as well as the corresponding positive and negative slope intersection points close to the peak around 1065 nm.

The frequency chirp was measured with a repeated 10 Gbps 11100100 NRZ bit sequence generated with a 1 V peak-to-peak modulation voltage applied to the VCSEL biased at 4 mA. An optical isolator was used to prevent feedback to the VCSEL from the etalon. As shown in [24], the time dependence of the frequency chirp, $\Delta f(t)$, can be calculated from the waveforms $V^+(t)$ and $V^-(t)$ as

$$\Delta f(t) \approx \frac{\dfrac{V^+(t) - V^-(t)}{V^+(t) + V^-(t)}}{\dfrac{2\pi}{FSR}\sqrt{(1-T_0)\left[T_0\dfrac{(1+R)^2}{(1-R)^2} - 1\right]}}, \quad (2)$$

where $V^+(t)$ is the waveform captured when the laser wavelength is tuned to the mid-point of the positive slope and $V^-(t)$ is the waveform captured when the laser wavelength is tuned to the mid-point of the negative slope. T_0 is the mid-point transmission of the etalon. The waveforms were captured using a New Focus 1414 MM photodetector and an Agilent 86100C wide-bandwidth oscilloscope. The laser wavelength was tuned by varying the temperature. The ~0.4 nm tuning needed move the laser wavelength between the mid-points of the positive and negative slopes required a temperature change of ~5°C, which is expected to have a minor effect on VCSEL dynamics.

Fig. 8 shows the waveforms of intensity and frequency chirp over the duration of the bit sequence. As expected, the intensity waveform exhibits damped relaxation oscillations at the transients, whereas the chirp waveform shows the associated frequency fluctuations. The measured frequency chirp is +8 GHz at transitions from 0 to 1 and -15 GHz at

transitions from 1 to 0. The smaller frequency chirp at the turn-on transient is consistent with the larger damping at high excitation levels.

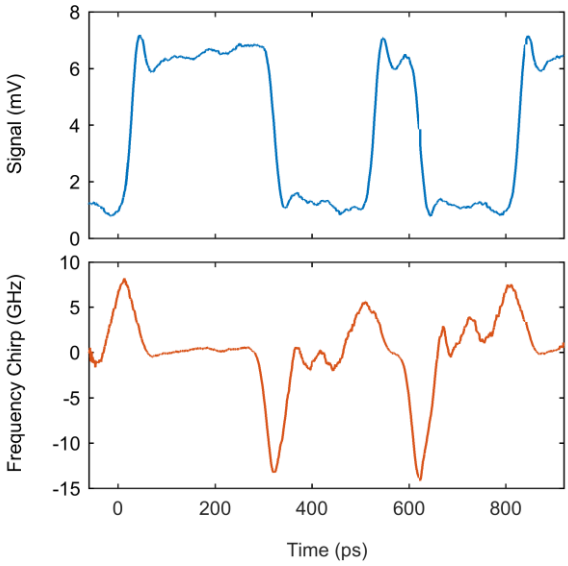

Fig. 8. Time-resolved signal measured with the VCSEL wavelength tuned to the positive transmission slope mid-point of the etalon (top), and VCSEL frequency chirp (bottom), obtained under 1 V peak-to-peak modulation using the 8-bit sequence 11100100.

V. Transmission Experiments

The 1060 nm SM VCSEL performance under large-signal modulation was investigated by data transmission in a BTB configuration, whereas the SM VCSEL and SMF link performance was investigated with fiber lengths of 1 and 2 km. Since the use of an SMF implies a more demanding alignment to the VCSEL, we first investigate the SM VCSEL-to-SMF coupling efficiency and alignment tolerance. Finally, we perform a theoretical analysis of the chirp-induced pulse compression/broadening using the measured time-bandwidth product of a short optical pulse from the VCSEL and chromatic dispersion data for the fiber.

A. Fiber Properties

The 1060 nm SMF used in the following long reach transmission experiments was a prototype fiber manufactured by Corning. It was designed to have a cable cutoff less than 1000 nm, which ensures SM transmission at 1060 nm. The chromatic dispersion at 1060 nm is close to -31 ps/nm/km, which is a factor of three lower than the value at 850 nm. At 1060 nm, the SMF has a 7.6 µm mode-field diameter (MFD) and a numerical aperture of 0.11. The attenuation is 0.77 dB/km, which is less than half the attenuation at 850 nm.

B. Fiber Coupling

For maximum coupling efficiency, the VCSEL near-field was projected on the fiber end face using an anti-reflection coated lens system. The launch conditions were optimized by matching the VCSEL beam size to the fiber MFD. The fiber was also held at a slight angle to eliminate optical feedback to the VCSEL. The VCSEL beam waist diameter, deduced from the beam measurements, is 2.6 µm at a bias current of 4 mA. Therefore, a 3-times magnification was used to couple the VCSEL output to the SMF. The alignment tolerance was measured by precise movement of the fiber in the transverse plane using a piezoelectric positioner and recording the output power at the other end of the 1 km long fiber. The fiber-coupled power was calculated by accounting for the fiber attenuation of 0.77 dB/km at 1060 nm, and is presented in terms of coupling efficiency in Fig. 9. The peak coupling efficiency is 73% and the -3 dB alignment tolerance is ±2.7 µm.

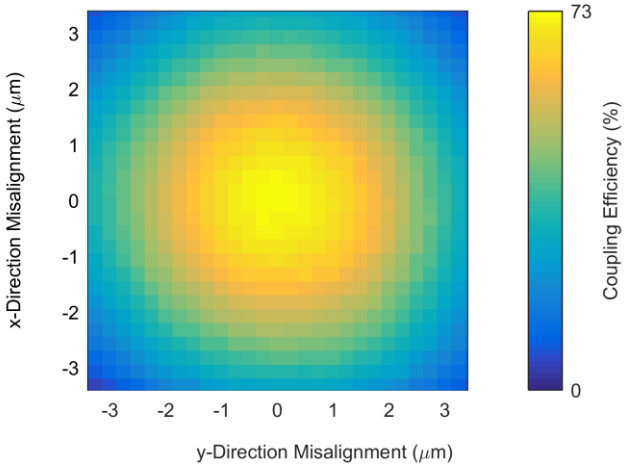

Fig. 9. Fiber-coupled power versus radial misalignment between the VCSEL and the SMF tip, obtained from measurements performed over 1 km of fiber.

C. Data Transmission

Transmission experiments were performed with data generated by an SHF 12103A bit pattern generator and amplified by a 55 GHz SHF 804TL amplifier to create a 1 V peak-to-peak, OOK-NRZ, PRBS15 drive signal. The VCSEL was biased at 4 mA and modulated by the drive signal through a 40 GHz bias tee and a 40 GHz ground-signal-ground wafer probe (Picoprobe). The optical output was coupled to fibers of varying length using the 3-times magnifying lens system, and then optically attenuated before the receiver. The signal was received by a 32 GHz Picometrix PT-28B linear photoreceiver and assessed by an SHF 11100B error analyzer to quantify the bit-error-ratio (BER). Given a start time delay and voltage threshold, the error analyzer was set to automatically align the edges of the gate signal, corresponding to a given BER limit, to the incoming continuous PRBS data. Eye diagrams of the received signals were recorded using an Agilent 86100C 70 GHz equivalent time sampling oscilloscope. In the BTB configuration, a 1 m OM4 fiber was used. For the long-reach transmission experiments, the SMF with lengths of 1 and 2 km was used.

Eye diagrams and BERs for each of the fiber lengths are shown in Fig. 10 and Fig. 11, respectively. Error-free transmission (BER < 10^{-12}, with >95% confidence) is achieved at both 25 and 40 Gbps over 1 and 2 km of the 1060 nm SMF, as well as in the BTB configuration. At the lower data rate of

25 Gbps, there is no noticeable OMA (optical modulation amplitude) penalty when increasing the distance. However, under 40 Gbps modulation, an improvement is observed with a negative penalty of 3 dB when comparing 1 km of SMF to BTB. From 1 to 2 km there is a positive penalty of 2 dB. This is due to pulse compression followed by pulse broadening with increasing length of fiber because of the negative fiber chromatic dispersion at 1060 nm. The extinction ratio was measured to be 6.8, 6.7 and 6.6 dB for BTB, 1 km and 2 km, respectively. The VCSEL energy dissipation at the 40 Gbps data rate is 240 fJ/bit.

Skewing of the eye after propagation over fiber is also observed in Fig. 10. This is a result of the negative fiber dispersion (positive group velocity dispersion parameter) and the positive (negative) transient chirp at the leading (trailing) edges of the bit stream (Fig. 8). The larger chirp at the trailing edge, together with the adiabatic chirp, causes a larger reduction of the fall time than the rise time, and therefore skew [25].

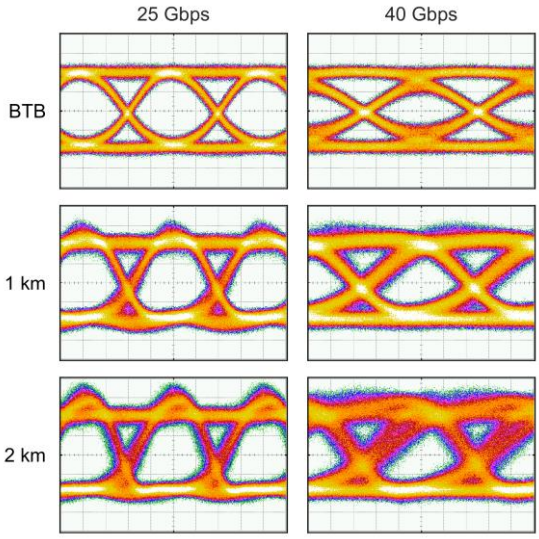

Fig. 10. Eye diagrams of received signals (25 mV/div) from large-signal modulation experiments with the SM VCSEL, biased at 4 mA, undergoing 1 V peak-to-peak OOK-NRZ modulation at 25 and 40 Gbps, for transmission BTB (1 m OM4), and over 1 and 2 km of 1060 nm SMF.

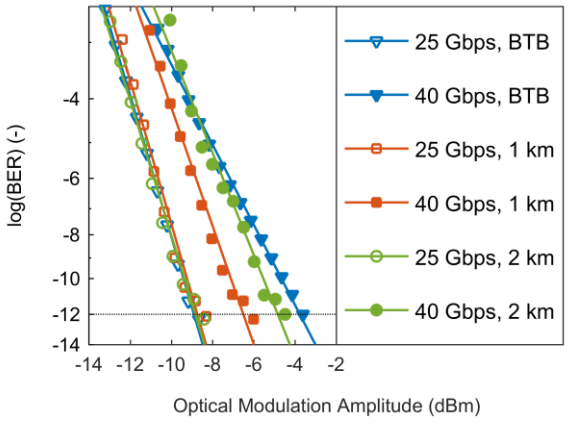

Fig. 11. BER versus OMA at 25 and 40 Gbps for links with a short OM4 fiber (BTB) and 1 and 2 km SMF.

The transmission experiments were performed without equalization, FEC or other forms of digital signal processing (DSP). Pre-emphasis of the drive signal should enable error-free 50 Gbps transmission over 2 km, as suggested by the recent demonstration of 50 Gbps transmission over 1 km using a simple form of pre-emphasis [26].

D. Chirp Induced Penalty

To understand the chirp induced penalty and its dependence on fiber length we use the theory in [27] for pulse compression and broadening along a dispersive fiber, which provides the following relation between the pulse width T_1 at propagation distance z and the pulse width T_0 at the input (assuming a chirped Gaussian pulse)

$$\frac{T_1}{T_0} = \sqrt{\left(1+\frac{C\beta z}{T_0^2}\right)^2 + \left(\frac{\beta z}{T_0^2}\right)^2}, \qquad (3)$$

where C is the chirp parameter and β is the group velocity dispersion parameter, which is related to the fiber chromatic dispersion. In [26], from the measured time-bandwidth product of a short optical pulse emitted by the SM VCSEL, the chirp parameter was determined to be 2.1.

Fig. 12 shows the dependence of pulse width on propagation distance and reveals initial pulse compression followed by pulse broadening due to the negative fiber dispersion at this wavelength. With a fiber chromatic dispersion of -31 ps/nm/km, we find a minimum pulse width at a distance of ~1.5 km, in fair agreement with the measured dependence of required OMA on fiber length (Fig. 11). Minimum pulse width at a distance of 2 km would require a fiber chromatic dispersion of -23 ps/nm/km.

VI. Conclusion

Optical links with a 1060 nm SM VCSEL and 1060 nm SMFs have been assembled to demonstrate up to 40 Gbps error-free OOK-NRZ transmission over 2 km (80 Gbps·km bitrate-distance product), without equalization, FEC, or other forms of DSP. Transmitter pre-emphasis should enable 50 Gbps transmission over the same distance. The results

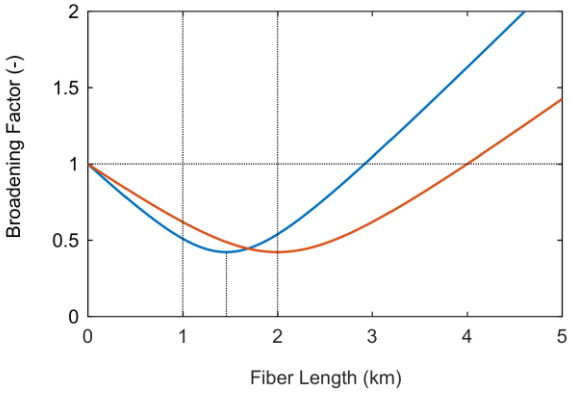

Fig. 12. Pulse broadening factor (T_1/T_0) versus fiber length with C from time-bandwidth measurements [25] and a fiber chromatic dispersion of -31 ps/nm/km (blue) and -23 ps/nm/km (red).

suggest that the GaAs-based VCSEL technology could potentially bring the same advantages in terms of cost and power efficiency to long-reach SM OIs as it has done to short-reach MM OIs at 850 nm.

The 1060 nm SM VCSEL, with a threshold current of 0.15 mA, a slope efficiency of 0.5 W/A, a beam divergence of 30° (full-width at $1/e^2$), and a 50 dB suppression of higher order transverse modes, was characterized with respect to all performance parameters of importance for data transmission. The maximum coupling efficiency to the SMF is 73%, with a -3 dB alignment tolerance of ±2.7 µm. At the bias current of 4 mA used for data transmission, the output power is 1.7 mW, the differential resistance is 250 Ω, the modulation bandwidth is 22.1 GHz, and the average RIN is -157 dB/Hz. Time resolved frequency chirp measurements revealed a +8 GHz frequency shift at the turn-on transients and a -15 GHz shift at the turn-off transients. When propagating data over the SMF, this, together with the negative fiber chromatic dispersion at 1060 nm (-31 ps/nm/km), leads to an initial pulse compression and a negative power penalty, followed by pulse broadening and a positive power penalty. A theoretical analysis showed maximum pulse compression at a fiber length of 1.5 km. Maximum compression at a fiber length of 2 km would require a fiber chromatic dispersion of -23 ps/nm/km with this particular SM VCSEL.

REFERENCES

[1] J. A. Tatum, D. Gazula, L. A. Graham, J. K. Guenter, R. H. Johnson, J. King, C. Kocot, G. D. Landry, I. Lyubomirsky, A. N. MacInnes, E. M. Shaw, K. Balemarthy, R. Shubochkin, D. Vaidya, M. Yan and F. Tang, "VCSEL-based interconnects for current and future data centers," *IEEE J. Lightwave Technol.*, vol. 33, no. 4, pp. 727-732, Feb. 2015, DOI. 10.1109/JLT.2014.2370633.

[2] M.-J. Li, "MMF for high data rate and short length applications," in *Proc. OFC*, San Francisco, CA, USA, 2014, paper M3F.1, DOI. 10.1364/OFC.2014.M3F.1.

[3] Y. Sun, "Recent advances for high speed short reach optical interconnects for datacom links," in *Proc. ICSJ*, Kyoto, Japan, 2017, pp. 63-65, DOI. 10.1109/ICSJ.2017.8240089.

[4] G. Denoyer, C. Cole, A. Santipo, R. Russo, C. Robinson, L. Li, Y. Zhou, J. Chen, B. Park, F. Boeuf, S. Crémer and N. Vulliet, "Hybrid silicon photonic circuits and transceiver for 50 Gb/s NRZ transmission over single-mode fiber," *IEEE J. Lightwave Technol.*, vol. 33, no. 6, pp. 1247-1254, Mar. 2015, DOI. 10.1109/JLT.2015.2397315.

[5] H. Yamazaki, S. Kanazawa, Y. Nakanishi, Y. Ueda, W. Kobayashi, Y. Muramoto, H. Ishii, and H. Sanjoh, "Ultra-broadband EA-DFB laser module for 200 Gbit/s PAM4 transmitter", *Proc. OFC*, Los Angeles, CA, USA, 2017, paper Th4G.3, DOI. 10.1364/OFC.2017.Th4G.3.

[6] D. M. Kuchta, T. N. Huynh, F. E. Doany, L. Schares, C. W. Baks, C. Neumeyr, A. Daly, B. Kögel, J. Rosskopf and M. Ortsiefer, "Error-free 56 Gb/s NRZ modulation of a 1530-nm VCSEL link," *IEEE J. Lightwave Technol.*, vol. 34, no. 14, pp. 3275-3282, Jul. 2016, DOI. 10.1109/JLT.2016.2552220.

[7] Ethernet Alliance, The 2018 Ethernet Roadmap, 2018. [Online]. Available: http://ethernetalliance.org/the-2018-ethernet-roadmap

[8] H. Hatakeyama, T. Anan, K. Fukatsu, N. Suzuki, K. Tokutome and M. Tsuji, "Highly reliable high-speed 1.1 µm range VCSELs with InGaAs/GaAsP MQW," *IEEE J. Quantum Electron.*, vol. 46, no. 6, pp. 890-897, Jun. 2010, DOI. 10.1109/JQE.2010.2040583.

[9] J. Guenter, B. Hawkins, R. Hawthorne and G. Landry, "Reliability of VCSELs for >25Gb/s," *Proc. OFC*, San Francisco, CA, USA, 2014, paper M3G.2, DOI. 10.1364/OFC.2014.M3G.2.

[10] K. Nagashima, T. Kise, Y. Ishikawa and H. Nasu, "A record 1-km MMF NRZ 25.78-Gb/s error-free link using a 1060-nm DIC VCSEL," *IEEE Photon. Technol. Lett.*, vol. 28, no. 4, pp. 418-420, Feb. 2016, DOI. 10.1109/LPT.2015.2496912.

[11] S. K. Pavan, J. Lavrencik and S. E. Ralph, "VCSEL-based PAM-4 links up to 62 Gbit/s over OM3, OM4, and WB-MMF: Performance comparison at 850 nm and 1050 nm," *IEEE J. Lightwave Technol.*, vol. 35, no. 9, pp. 1614-1623, May 2017, DOI. 10.1109/JLT.2016.2647203.

[12] M. R. T. Tan, P. Rosenberg, W. V. Sorin, B. Wang, S. Mathai, G. Panotopoulos and G. Rankin, "Universal photonic interconnect for data centers," *IEEE J. Lightwave Technol.*, vol. 36, no. 2, pp. 175-180, Jan. 2018, DOI. 10.1109/JLT.2017.2747501.

[13] A. Larsson, E. Simpanen, J. S. Gustavsson, E. Haglund, E. P. Haglund, T. Lengyel, P. A. Andrekson, W. V. Sorin, S. Mathai, M. R. Tan and S. R. Bickham, "1060 nm VCSELs for long-reach optical interconnects," *Opt. Fiber Technol.*, vol. 44, pp. 36-42, Aug. 2018, DOI. 10.1016/j.yofte.2018.01.001.

[14] E. Simpanen, J. S. Gustavsson, E. Haglund, E. P. Haglund, A. Larsson, W. V. Sorin, S. Mathai and M. R. Tan, "1060 nm single-mode vertical-cavity surface-emitting laser operating at 50 Gbit/s data rate," *Electron. Lett.*, vol. 53, no. 13, pp. 869-871, Jun. 2017, DOI. 10.1049/el.2017.1165.

[15] E. Simpanen, J. S. Gustavsson, A. Larsson, W. V. Sorin, S. Mathai, M. R. Tan and S. R. Bickham. "Long-reach 1060 nm SM VCSEL - SMF optical interconnects," *Proc. ECOC*, Rome, Italy, 2018, paper Mo4I.6, DOI. 10.1109/ECOC.2018.8535524.

[16] E. Haglund, P. Westbergh, J. S. Gustavsson, E. P. Haglund and A. Larsson, "High-speed VCSELs with strong confinement of optical fields and carriers," *IEEE J. Lightwave Technol.*, vol. 34, no. 2, pp. 269-277, Jan. 2016, DOI. 10.1109/JLT.2015.2458935.

[17] E. P. Haglund, P. Westbergh, J. S. Gustavsson and A. Larsson, "Impact of damping on high-speed large signal VCSEL dynamics," *IEEE J. Lightwave Technol.*, vol. 33, no. 4, pp. 795-801, Feb. 2015, DOI. 10.1109/JLT.2014.2364455.

[18] P. Westbergh, J. S. Gustavsson, B. Kögel, Å. Haglund and A. Larsson, "Impact of photon lifetime on high-speed VCSEL performance," *IEEE J. Sel. Top. Quantum Electron.*, vol. 17, no. 6, pp. 1603-1613, Nov./Dec. 2011, DOI. 10.1109/JSTQE.2011.2114642.

[19] J. Gustavsson, Å. Haglund, J. Bengtsson, and A. Larsson, "High-speed digital modulation characteristics of oxide-confined vertical-cavity surface-emitting lasers – numerical simulations consistent with experimental results", *IEEE J. Quantum Electron.*, vol. 38, no. 8, pp. 1089-1096, Aug. 2002, DOI. 10.1109/JQE.2002.801009.

[20] H. Li, P. Wolf, J. A. Lott and D. Bimberg, "Relative intensity noise of temperature-stable, energy-efficient 980 nm VCSELs," *AIP Advances*, vol. 7, no. 2, Feb. 2017, DOI. 10.1063/1.4974258.

[21] T. Lengyel, K. Szczerba, E. P. Haglund, P. Westbergh, M. Karlsson, A. Larsson and P. A. Andrekson, "Impact of damping on 50 Gbps 4-PAM modulation of 25G class VCSELs," *IEEE J. Lightwave Technol.*, vol. 35, no. 19, pp. 4203-4209, Oct. 2017, DOI. 10.1109/JLT.2017.2727549.

[22] L.-G. Zei, S. Ebers, J.-R. Kropp and K. Petermann, "Noise performance of multimode VCSELs," *IEEE J. Lightwave Technol.*, vol. 19, no. 6, pp. 884-892, Jun. 2001, DOI. 10.1109/50.927523.

[23] J. Y. Law, G. P. Agrawal, "Effects of optical feedback on static and dynamic characteristics of vertical-cavity surface-emitting lasers," *IEEE J. Sel. Top. Quantum Electron.*, vol. 3, no. 2, pp. 353-358, Apr. 1997, DOI. 10.1109/2944.605678.

[24] S. Tammela, H. Ludvigsen, T. Kajava and M. Kaivola, "Time-resolved frequency chirp measurement using a silicon-wafer etalon," *IEEE Photon. Technol. Lett.*, vol. 9, no. 4, pp. 475-477, Apr. 1997, DOI. 10.1109/68.559393.

[25] P. Krehlik, "Directly modulated lasers in negative dispersion fiber links," *Opto-Electron. Review*, vol. 15, no. 2, pp. 71-77, Jun. 2007, DOI. 10.2478/s11772-007-0002-z.

[26] T. Lengyel, E. Simpanen, J. S. Gustavsson, A. Larsson, M. Karlsson, P. A. Andrekson, W. V. Sorin, S. Mathai, M. R. Tan and S. R. Bickham, "Pre-emphasis enabled 50 Gbps transmission over 1000 m SMF using a 1060 nm single-mode VCSEL," *Electronics Lett.*, vol. 54, no. 20, pp. 1186-1187, Oct. 2018, DOI. 10.1049/el.2018.6170.

[27] G. P. Agrawal, "Optical fibers," in *Fiber-Optic Communications Systems*, 3rd ed., New York, NY, USA, John Wiley & Sons Inc., 2002, ch. 2, sec. 2.3-2.4, pp. 38-50.